metallic complexes incorporated/immobilized in different solid supports, such as silica,[21] polymeric fibers,[22] mesoporous titania,[20] alumina aerogels and xerogels,[23] zeolites,[24] as well as fullerene-based nanoconjugates[25] and, more recently, a 3D graphene oxide foam.[26] Li *et al.* describe the application of thiolate-stabilized gold nanoclusters in the sulfoxidation of different organic sulfides.[27] The nanoclusters showed interesting catalytic activity in the sulfoxidation of thioanisole using iodosylbenzene as the oxidant with no significant loss of activity after five consecutive cycles.

The oxidation of styrene is of great importance for the industry since the main products obtained, *i.e.* styrene oxide and benzaldehyde, are valuable organic intermediates for the production of fine chemicals. Environmentally friendly methods for oxidation of styrene with a clean oxidant have been the subject of current research.[28–33] The application of metallic nanoparticles to catalyze styrene oxidation in the presence of hydrogen peroxide is not largely explored. The few work performed is based on iron oxide[32] and titanium dioxide[34] supported in silica matrices and more recently in gold and silver nanoparticles incorporated in layered manganese oxides.[31] The application of MOFs as heterogeneous catalysts for styrene oxidation has been investigated mainly in the presence of organic oxidants such as *tert*-butyl hydroperoxide, among others.[35–37] Using sustainable oxidants, such as hydrogen peroxide, scarce work can be find in the literature.[30,38,39]

In this work we report the preparation of the first hybrid composites based on $CoAl_2O_4$ nanoparticles obtained through their incorporation within the porous framework of MIL-101(Cr). Different sized nanoparticles were selected, with average diameters of approximately 5.5 nm and 2.5 nm which led to the formation of the CoAl-1@MIL(Cr) and CoAl-2@MIL(Cr) composites, respectively. The novel composites presented a remarkable catalytic activity for the sulfoxidation of thioanisole under sustainable conditions. The catalytic application of CoAl-1@MIL(Cr) was enlarged to the oxidation of styrene. The influence of the nanoparticles size in the catalytic performance was evaluated. The catalytic efficiency, robustness and recycling ability of the composites was investigated. To the best of our knowledge, this is the first work reporting the incorporation of $CoAl_2O_4$ nanoparticles in MOF-type materials for catalytic applications.

Results and discussion

Catalyst preparation and characterization

The composite materials were prepared through the incorporation of $CoAl_2O_4$ nanoparticles with average sizes of 5.5 nm and 2.5 nm in the chromium terephthalate MIL-101(Cr) framework resulting in the composites CoAl-1@MIL(Cr) and CoAl-2@MIL(Cr), respectively. These materials were extensively characterized by several techniques, including elemental analysis, vibrational spectroscopy (FT-IR and FT-Raman), powder X-ray diffraction (XRD), scanning electron microscopy (SEM), transmission electron microscopy (TEM) and energy dispersive X-ray spectroscopy (EDX). The elemental analysis results indicate the presence of Co and Al from the nanoparticles with a total metal loading of 2.0 wt% and 0.54 wt% for CoAl-1@MIL(Cr) and CoAl-2@MIL(Cr), respectively. The FT-IR spectra of the composites were compared with the spectra of the MIL-101(Cr) support and the $CoAl_2O_4$ nanoparticles (Fig. 1A and S1, ESI†). The spectra are mainly composed by the typical absorption bands of the solid support, namely the intense bands in the 1700–1300 cm^{-1} range assigned to ν_{as}(COO), ν_s(COO) and ν(C–C).[40,42] Other typical bands can also be found in both spectra, such as the less intense bands ascribed to the δ(C–H) and γ(C–H) stretching modes of the aromatic rings[40] located at *ca.* 1018; 748 cm^{-1} and 991; 721 cm^{-1} for CoAl-1@MIL(Cr) and CoAl-2@MIL(Cr), respectively. Some evidences, however, can be found regarding the presence of the nanoparticles in the final composite specially in the CoAl-1@MIL(Cr) spectrum. It is possible to observe an increase of the relative intensity of some bands, namely the bands located at 1620 and 1018 cm^{-1}, when compared with the same bands in the MIL-101(Cr) spectrum.

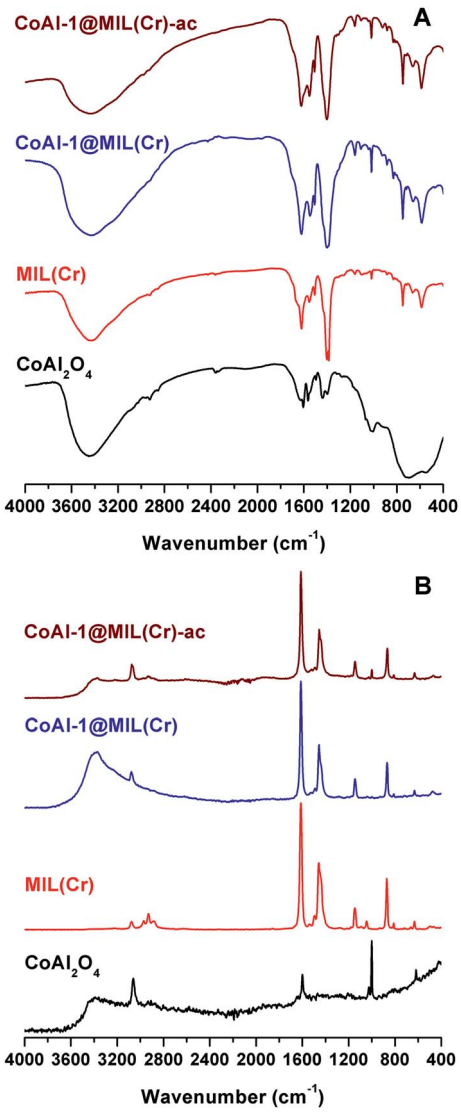

Fig. 1 FT-IR (A) and FT-Raman (B) spectra of $CoAl_2O_4$ nanoparticles, the solid support MIL-101(Cr) and the CoAl-1@MIL(Cr) composite before and after catalysis.

Such fact is most likely due to the relative contribution of the nanoparticles bands that leads to the increase of the MIL-101 bands located at similar wavenumbers in the CoAl-1@MIL(Cr) spectrum. The FT-Raman spectrum of CoAl-1@MIL(Cr) (Fig. 1B) exhibits the characteristic bands arising from the MOF.[43] The presence of the nanoparticles in the composite is shown by a broad band (3377 cm^{-1}) assigned to the ν(O–H) of water molecules together with a band located at *ca.* 3078 cm^{-1} attributed to the ν(C–H) of the phenyl rings arising from the solvent used in the nanoparticles preparation.[44] The spectrum of CoAl-2@MIL(Cr) (Fig. S2, ESI†) is nearly identical to the MIL-101(Cr), although in this case the presence of the nanoparticles is not so clear probably as a result of the lower metal loading in this composite.

The isolated nanoparticles, the MIL-101(Cr) support and the composite materials were studied by powder XRD (Fig. 2 and S3, ESI†). In the patterns of both composites, the main diffraction peaks of the MOF [for example, $2\theta = 3.99$ (h, k, l, 4, 0, 0), 5.20 (3, 3, 3), 5.84 (5, 3, 1), 8.40 (6, 6, 0), 9.00 (7, 5, 3) and 10.40 (10, 2, 2)] remain essentially unaltered after the incorporation of the nanoparticles. This fact indicates that the crystalline structure of MIL-101(Cr) is retained in the final composite materials and no collapse or degradation of the framework occurs. The absence of peaks from the nanoparticles in the CoAl-1@MIL(Cr) and CoAl-2@MIL(Cr) XRD patterns suggests a dispersion of the nanoparticles within the frameworks. In fact, the XRD patterns of the composites are dominated by the peaks of the more crystalline and abundant MOF while the broad and low intensity peaks of the nanoparticles are probably hidden in the background.

The morphology and chemical composition of the composite materials was also assessed by electron microscopy and energy dispersive X-ray spectroscopy (EDX). For comparison purposes, the isolated nanoparticles and the solid support were also studied by electron microscopy. The SEM images (Fig. S4, ESI†) of the composite materials show the characteristic morphology of the solid support although the presence of the nanoparticles is not clear. Fig. 3a shows the HRTEM image of the $CoAl_2O_4$ nanoparticles with an average size of 5.5 nm exhibiting a good dispersion and a uniform quasi-spherical morphology. The HRTEM image of the solid support (Fig. 3b) shows very well-defined cubic micro-crystals which are typical of the MIL-101(Cr) morphology[15] while the corresponding EDX spectrum (not shown) reveals the presence of Cr. The higher resolution obtained with the HRTEM technique allowed to observe the presence of the nanoparticles in the composite. In fact, the HRTEM images of CoAl-1@MIL(Cr) (Fig. 3c and d) exhibits the $CoAl_2O_4$ nanoparticles supported on the cubic micro-crystals of the solid support. Furthermore, the existence of cobalt and aluminum in the EDX spectrum (Fig. S5a, ESI†) unequivocally confirms the presence of the $CoAl_2O_4$ nanoparticles in the composite material.

EDX elemental mapping was also performed for the CoAl-1@MIL(Cr) composite (Fig. 4). The results indicate a uniform distribution of chromium from MIL-101(Cr) as well as the existence of the nanoparticles in the composite by showing the presence of the cobalt and aluminum elements.

Catalytic studies

The composite materials were evaluated as heterogeneous catalysts in the oxidation of thioanisole (**i**, Scheme 1). The CoAl-1@MIL(Cr) composite was also tested in the oxidation of styrene (**iv**, Scheme 1). Acetonitrile was used as the solvent and H_2O_2 or aqueous *t*-BuOOH were used as oxidants in the oxidation of thioanisole (**i**) and styrene (**iv**), respectively. No conversion was observed using only the isolated solid support (MIL-101(Cr)) in similar catalytic conditions to the ones used in

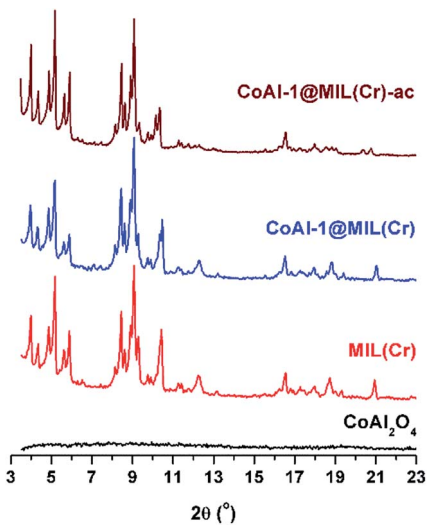

Fig. 2 Powder XRD patterns of $CoAl_2O_4$ nanoparticles, the solid support MIL-101(Cr) and the CoAl-1@MIL(Cr) composite before and after catalysis in the 3 23° range.

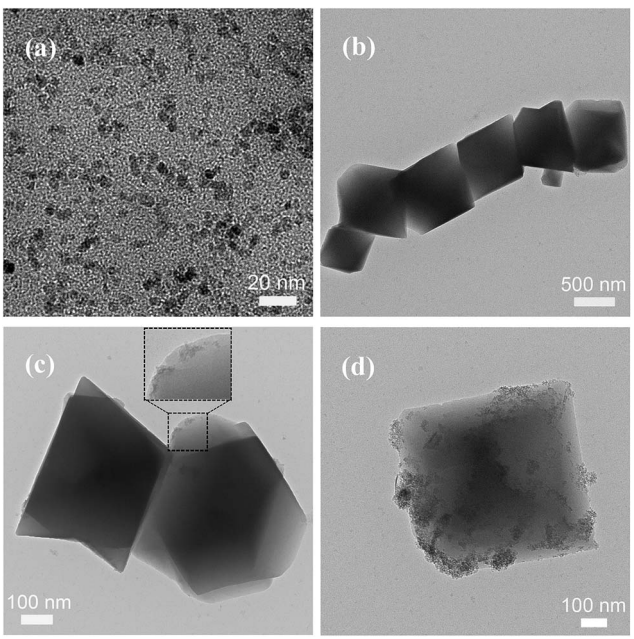

Fig. 3 HRTEM images of (a) $CoAl_2O_4$ nanoparticles, (b) solid support MIL-101(Cr), (c) and (d) CoAl-1@MIL(Cr) composite material.

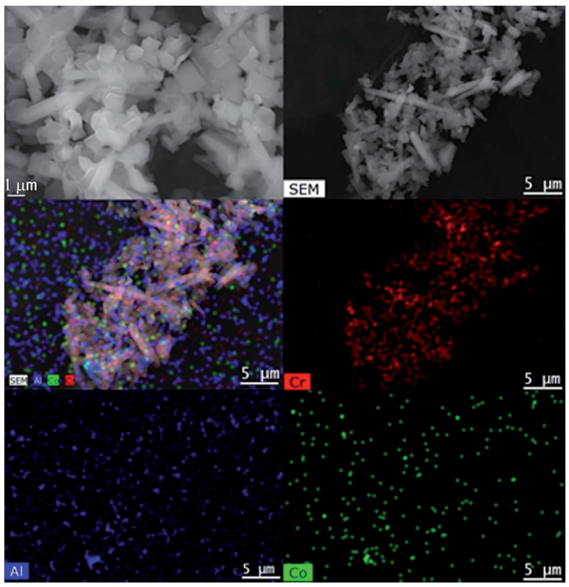

Fig. 4 SEM image and elemental mapping images for CoAl-1@MIL(Cr) composite material.

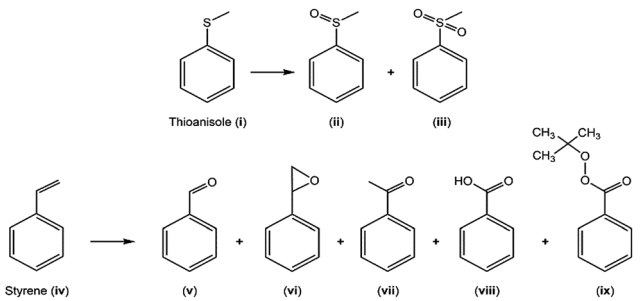

Scheme 1 Schematic representation of the oxidation products for the different substrates.

the oxidation reactions. The catalytic results obtained are summarized in Tables 1 and 2 for the oxidations of thioanisole (**i**) and styrene (**iv**), respectively. Fig. 5 compares the kinetic profiles obtained for the oxidation of thioanisole (**i**) catalyzed by CoAl-1@MIL(Cr) and CoAl-2@MIL(Cr). These reactions were performed using the same percentage of $CoAl_2O_4$ active centers [6 mg of CoAl-1@MIL(Cr) and 20 mg CoAl-2@MIL(Cr)] in both composites to investigate the influence of the nanoparticle size. It is possible to observe that the composite incorporating the larger size $CoAl_2O_4$ nanoparticles, CoAl-1@MIL(Cr), presented higher conversions in shorter reaction times. This is an unexpected result since it is well known that the nanoparticles with smaller dimensions usually show higher conversion.[45] However, it is also known that the activity of the nanoparticles is largely influenced by the nature of the support.[45] Since the support in both composites is the same (MIL-101(Cr)) and it is absent of catalytic activity even in the presence of high amounts (*i.e.* 20 mg), the difference of activity observed between the composites may be related with the different loading obtained for each composite and, probably a different interaction of $CoAl_2O_4$

Table 1 Catalytic data for the oxidation of thioanisole[a] using the heterogeneous catalysts

			Selectivity[b] (%)	
	Time (h)	Conversion (%)	**ii**	**iii**
CoAl 1@MIL(Cr)				
1st cycle	0.17	46	70	30
	0.5	95	68	32
2nd cycle	0.17	45	42	58
	0.5	96	71	29
3rd cycle	0.17	44	80	20
	0.5	99	76	24
CoAl 2@MIL(Cr)				
1st cycle	0.17	42	48	52
	0.5	83	95	5
2nd cycle	0.17	86	100	
	0.5	94	100	
3rd cycle	0.17	97	100	
	0.5	98	100	

[a] Reaction conditions: 0.5 mmol of substrate, 2 mmol H_2O_2, 6 mg of CoAl 1@MIL(Cr) or 20 mg of CoAl 2@MIL(Cr), 1.0 mL CH_3CN at 70 °C. [b] Based on the amount of consumed substrate.

nanoparticles with the support and their stability inside the MIL-101(Cr) cavities. To further investigate this point, the oxidation of thioanisole using the isolated nanoparticles without the solid support was performed. The oxidation was carried out using equivalent amounts of nanoparticles to the ones present in the composite materials according to its metal loading. As expected, the smaller size nanoparticles (CoAl-2) exhibited a higher catalytic activity than the larger nanoparticles (CoAl-1). The comparison between the catalytic performance of the nanoparticles and the related composites (Fig. S6, ESI†) shows that the immobilization of the nanoparticles has led to an enhancement of their catalytic activity. This enhancement effect is more pronounced for the larger nanoparticles (CoAl-1) probably as a consequence of a higher

Table 2 Catalytic data for the oxidation of styrene[a] using the CoAl-1@MIL(Cr) heterogeneous catalyst

			Selectivity[b] (%)				
	Time (h)	Conversion (%)	**v**	**vi**	**vii**	**viii**	**ix**
CoAl 1@MIL(Cr)							
1st cycle	2	8	50	50			
	6	26	42	54			4
	30	89	48	33	6	3	10
2nd cycle	2	8	50	50			
	6	21	43	57			
	30	87	39	34	8	5	14
3rd cycle	2	8	88	13			
	6	22	73	27			
	30	93	33		11	1	55

[a] Reaction conditions: 1 mmol of substrate, 4.5 mmol *t* BuOOH, 20 mg of catalyst, 1.5 mL CH_3CN at 70 °C. [b] Based on the amount of consumed substrate.

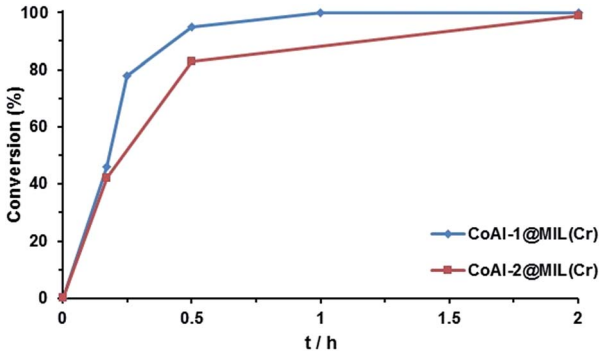

Fig. 5 Kinetic profile for the oxidation of thioanisole using CoAl-1@MIL(Cr) and CoAl-2@MIL(Cr) heterogeneous catalysts.

nanoparticle loading. In fact, the higher nanoparticle loading of CoAl-1@MIL(Cr) composite when compared with that of CoAl-2@MIL(Cr) may be responsible for the different conversion values observed. In CoAl-1@MIL(Cr), the higher number of catalytic active centers present per cavity of MIL-101(Cr) could result in a more pronounced confinement effect.[39,46] In this case, more frequent interactions between the active centers and the substrates will occur which could lead to higher conversion values.

For the oxidation of thioanisole (**i**), a practically complete conversion (95%) was attained using CoAl-1@MIL(Cr) after only 30 min of reaction with 68% of selectivity towards methylphenylsulfoxide (**ii**). For the same reaction time, using CoAl-2@MIL(Cr) has led to a 83% conversion and 95% selectivity towards methylphenylsulfoxide (**ii**). Some examples can be found in the literature dealing with the oxidation of thioanisole catalyzed by metallic nanoparticles.[27,47,48] Despite reporting practically complete conversions in the oxidation of thioanisole, the catalysts require much longer reactions times than the CoAl-*x*@MIL(Cr) composites herein reported. Although having a higher surface area, the smaller nanoparticles (*ca.* 2.5 nm) in CoAl-2@MIL(Cr) have shown similar or even inferior catalytic activity than the nanoparticles (*ca.* 5.5 nm) in CoAl-1@MIL(Cr). The extremely fast reaction rate of this oxidation together with the confinement effect promoted by the cages of MIL-101(Cr) are probably responsible for the similar activity observed of both composites despite the different size of the nanoparticles.

The slightly better catalytic performance of the CoAl-1@MIL(Cr) composite has motivated its application in a different catalytic reaction, namely in the oxidation of styrene (**iv**). The use of CoAl-1@MIL(Cr) resulted in an 89% conversion after 30 h of reaction with 48% selectivity towards benzaldehyde (**v**). As shown in Table 2, after 2 h of reaction only benzaldehyde (**v**, 50%) and styrene oxide (**vi**, 50%) are formed. However, at the end of the reaction (30 h) other oxidation products are observed: acetophenone (**vii**, 6%), benzoic acid (**viii**, 3%) and *t*-butylperoxybenzoate (**ix**, 10%). Until the first 2 h of reaction, the only products obtained are benzaldehyde (**v**) and styrene oxide (**vi**) in approximately equal amounts. For this reason, the other oxidation products (acetophenone, benzoic acid and *t*-butylperoxybenzoate), that are only present after the initial 6 h of reaction, should be formed through the further oxidation of the first two oxidation products (benzaldehyde and styrene oxide). The gradual decrease in the selectivity values of benzaldehyde and styrene oxide after the initial 6 h of reaction, should indicate that the later oxidation products are probably formed through the subsequent oxidation of the two initial products. This reaction path is consistent with reports in the literature dealing with the oxidation of styrene using *t*-BuOOH as the oxidant. Choudhary *et al.* describe the oxidation of styrene using supported gold nanoparticles as heterogeneous catalysts.[49] In fact, the authors were able to conclude that benzaldehyde and styrene oxide are the primary products in the oxidation of styrene while the remaining products are formed through the oxidation of these primary products. Other publications reporting the catalytic oxidation of styrene with *t*-BuOOH as the oxidant also attribute the decrease in the selectivity of styrene oxide that usually occurs after long reactional times (>12 h) to its decomposition into benzaldehyde, acetophenone and benzoic acid.[50,51]

As previously performed, the catalytic activity of the isolated nanoparticles was also evaluated in the oxidation of styrene using identical experimental conditions. The results obtained reveal that the immobilization of the nanoparticles besides the advantage of allowing the recycling of the catalyst also enhances its catalytic performance towards the oxidation of styrene (Fig. S7, ESI†).

Recyclability and leaching

The recyclability of the composite materials was evaluated for the oxidative reactions previously described. After each catalytic cycle, the catalysts were recovered by centrifugation, washed thoroughly with acetonitrile and dried in a desiccator over silica gel. The solids were then reused in a new oxidation reaction using the same experimental conditions. The catalytic data for the second and third cycles is summarized in Tables 1 and 2 for the oxidation of thioanisole (**i**) and styrene (**iv**), respectively. Fig. 6 shows the conversion values obtained for three consecutive cycles in the oxidation of thioanisole (**i**) using CoAl-1@MIL(Cr). The kinetic profiles for the three cycles are practically similar. As shown in Table 1, the selectivity values

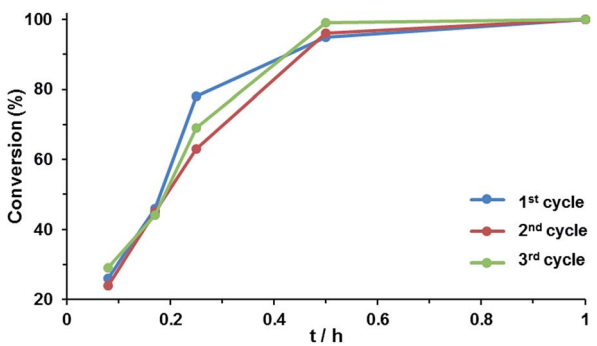

Fig. 6 Kinetic profile for three consecutive catalytic cycles for the oxidation of thioanisole using CoAl-1@MIL(Cr) as the catalyst.

throughout the catalytic cycles also remain essentially unaltered. In fact, besides the similar conversion values, the selectivity values for the two products formed, methylphenylsulfoxide (**ii**) and methylphenylsulfone (**iii**), are identical. The conversion values obtained with both composites in the oxidation of thioanisole (**i**) are very similar along the catalytic cycles (Fig. 7).

The CoAl-2@MIL(Cr) composite has shown a higher selectivity towards methylphenylsulfoxide (**ii**) throughout the three catalytic cycles than CoAl-1@MIL(Cr) (Fig. 8). The high reproducibility observed in all oxidative reactions clearly confirms the robustness and reusability of the heterogeneous catalysts in the oxidation of this substrate.

The reusability of CoAl-1@MIL(Cr) was also investigated for the oxidation of styrene (**iv**) in order to evaluate its versatility as heterogeneous catalyst. Fig. 9 exhibits the kinetic profiles for the oxidation of styrene with CoAl-1@MIL(Cr) and *t*-BuOOH for three consecutive cycles. The high recycling ability of the composite can be observed from the very similar kinetic profiles throughout the catalytic cycles. This similarity is consistent with a high robustness of the heterogeneous catalyst since it strongly indicates that no chemical decomposition/degradation occurs during the cycles. As shown in Table 2, conversion values of 87% or higher were achieved after 30 h of reaction in the three cycles. Fig. 10 compares the conversion and selectivity towards benzaldehyde (**v**) values obtained in the oxidation of styrene with *t*-BuOOH for three consecutive cycles. The conversion values along the catalytic cycles are similar, but there is a slight decrease in the selectivity along the catalytic cycles. In fact, while the major product obtained in the oxidation of styrene in the first two cycles is benzaldehyde (**v**), in the third cycle the main oxidation product is *t*-butylperoxybenzoate (**ix**). As previously discussed, this behavior is due to the decomposition of benzaldehyde and styrene oxide that occurs after long reactional times.

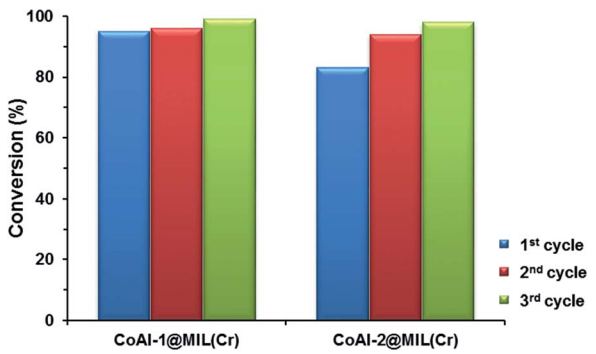

Fig. 7 Conversion data obtained for three consecutive cycles in the oxidation of thioanisole after 30 min of reaction using both catalysts.

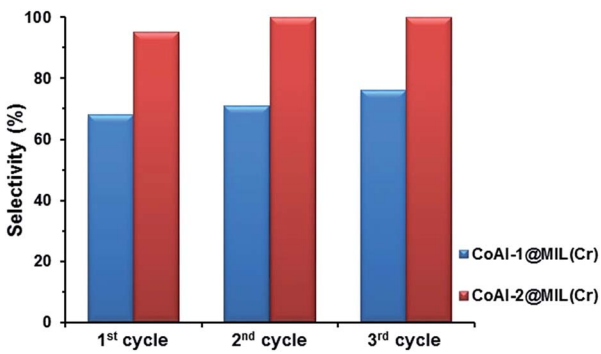

Fig. 8 Selectivity towards methylphenylsulfoxide (ii) obtained for the oxidation of thioanisole using both catalysts after 30 min of reaction.

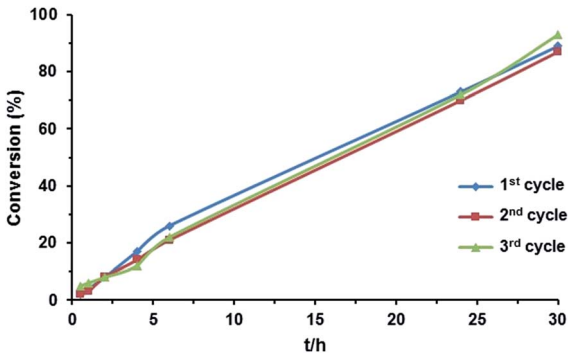

Fig. 9 Kinetic profile for three consecutive catalytic cycles for the oxidation of styrene using CoAl-1@MIL(Cr).

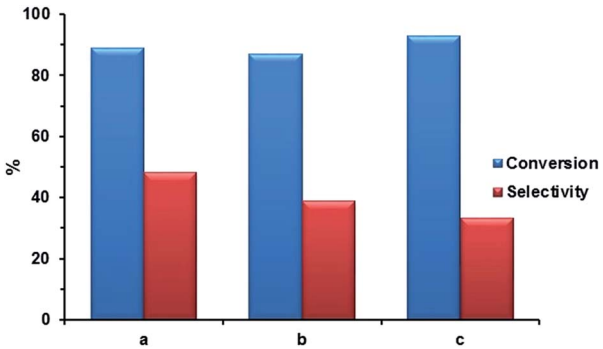

Fig. 10 Conversion and selectivity towards benzaldehyde (**v**) data obtained for the oxidation of styrene using CoAl-1@MIL(Cr) after 30 h for the (a) first, (b) second and (c) third cycles.

The CoAl-1@MIL(Cr) composite has shown to be an active and recyclable heterogeneous catalyst in both thioanisole and styrene oxidation reactions for three consecutive cycles. In particular, the composite exhibited a remarkable catalytic activity towards the thioanisole oxidation using H_2O_2 as the oxidant (conversions higher than 95% for 30 min of reaction) when compared with the majority of reports found in the literature. Walmsley *et al.* have reported the application of oxovanadium(IV)-functionalized polybenzimidazole nanofibres as heterogeneous catalyst in the oxidation of thioanisole exhibiting interesting catalytic activity and recyclability.[22] Similar conversion and selectivity values to our work were attained along three catalytic cycles, although for three times longer reaction times.

Catalyst material stability

The stability of the heterogeneous catalysts was investigated through the extensive characterization of the solid recovered after three consecutive cycles of thioanisole oxidation, CoAl-1@MIL(Cr)-ac (ac stands for after catalysis). The vibrational spectroscopy (Fig. 1) spectra of CoAl-1@MIL(Cr)-ac are very similar to the corresponding ones before catalysis. One exception is the appearance of the nanoparticles most intense band (1001 cm^{-1}) in the Raman spectrum of the composite after catalysis (Fig. 1B). This band is absent in the corresponding spectrum before catalysis as a result of the incorporation of the nanoparticles within the MIL-101 framework. Therefore, the appearance of this band in the spectrum after catalysis should be related with the occurrence of some leaching of the nanoparticles during the catalytic cycles. In fact, the elemental analysis results indicate a Al/Cr(wt%) ratio of 0.05 for CoAl-1@MIL(Cr)-ac which is slightly lower than the ratio obtained before catalysis (0.075). The XRD pattern of the composite after catalysis (Fig. 2) exhibits a very similar profile to the pattern of CoAl-1@MIL(Cr) regarding the position and intensity of the main peaks of MIL-101(Cr) suggesting that the MOF structure is preserved after the three catalytic cycles. The morphology of the composite seems to be preserved after the catalytic cycles as the SEM images of CoAl-1@MIL(Cr)-ac (Fig. S8, ESI†) still exhibit the characteristic cubic microcrystals of MIL-101(Cr). The EDX spectrum of CoAl-1@MIL(Cr)-ac (Fig. S5b, ESI†) also shows the presence of the elements that compose the nanoparticles (Co and Al) in a similar ratio to the EDX spectrum before catalysis. The stability of the $CoAl_2O_4$ nanoparticles was also evaluated by determining its size distribution (through HRTEM images analysis) in the CoAl-1@MIL(Cr) composite after three catalytic cycles of styrene oxidation. The average size of the nanoparticles before catalytic use was 4.7 ± 0.8 nm while the corresponding value after the catalytic cycles was 4.2 ± 0.6 nm. Such a result indicates that no significant nanoparticle aggregation occurs which is consistent with the highly reproducible kinetic profiles obtained in the three styrene oxidation cycles.

Conclusions

Novel hybrid composite materials, CoAl-*x*@MIL(Cr), were prepared through the incorporation of $CoAl_2O_4$ nanoparticles ($x = 1$ for 5.5 nm; $x = 2$ for 2.5 nm average sizes) within the MIL-101(Cr) framework. The successful incorporation of the nanoparticles and the structural preservation of the metal–organic framework was confirmed by a vast number of characterization techniques, including vibrational spectroscopy (FT-IR and FT-Raman), elemental analysis, powder XRD, transmission and scanning electron microscopy (TEM/SEM) and energy dispersive X-ray spectroscopy (EDX) elemental mapping. The composites were tested as heterogeneous catalysts in oxidative reactions, namely in the oxidations of thioanisole and styrene.

The composite materials have proved to be efficient catalysts for oxidative catalysis, specially in the oxidation of thioanisole with practically complete conversions achieved after only 30 min of reaction. The similar catalytic data (conversion and selectivity) obtained in three consecutive catalytic cycles clearly suggests a high recycling ability of the composites. In this work, the size of the nanoparticles seems not to significantly influence the catalytic performance of the composites. The integrity of CoAl-1@MIL(Cr) was confirmed after three consecutive catalytic cycles by different characterization techniques. Following the interesting catalytic activity and robustness exhibited by $CoAl_2O_4$-containing composites, we are currently interested in the design of novel composites through the encapsulation/intercalation of these nanoparticles in other solid supports and their evaluation as heterogeneous catalysts.

Experimental

Materials and methods

All the reagents used in the preparation of the composite materials, such as chromium(III) nitrate nonahydrate [$Cr(NO_3)_3 \cdot 9H_2O$, Aldrich], benzene-1,4-dicarboxylic acid ($C_8H_6O_2$, Aldrich), hydrofluoric acid (HF, Aldrich), cobalt acetate [$(CH_3CO_2)_2Co$, Aldrich], benzyl alcohol (C_7H_8O, Aldrich) and aluminium isopropoxide [$Al(OC_3H_7)_3$, Aldrich] were used as received without further purification. The reagents used in the catalytic studies, namely thioanisole (Aldrich), styrene (Aldrich), acetonitrile (Panreac), hydrogen peroxide 30% (H_2O_2, Riedel-de-Häen) and aqueous *tert*-butylhydroperoxide (*t*-BuOOH, Aldrich) were used as received without further purification.

Elemental analyses for Co, Al and Cr were performed by ICP-MS at the Central Laboratory of Analyses of the University of Aveiro. FT-IR spectra were obtained on a Jasco 460 Plus spectrometer using KBr pellets, while the FT-Raman spectra were acquired on a RFS-100 Bruker FT-spectrometer, equipped with Nd:YAG laser with a 1064 nm excitation wavelength and laser power set to 350 mW. Powder X-ray diffraction patterns were obtained at room temperature on a X'Pert MPD Philips diffractometer, equipped with an X'Celerator detector and a flat-plate sample holder in a Bragg-Brentano *para*-focusing optics configuration (45 kV, 40 mA). Intensity data were collected by the step-counting method (step 0.013°), in continuous mode, in the *ca.* $3 \leq 2\theta \leq 70°$ range. Scanning electron microscopy (SEM) images were acquired in a high resolution scanning electron microscope Hitachi SU-70 instrument working at 4 kV.

High resolution transmission electron microscopy (HRTEM) was performed using a JEOL 2200FS microscope with a field emission gun operating at 300 kV. The energy-dispersive X-ray spectroscopy (EDX) data were collected on a Hitachi S-4100 field emission gun tungsten filament instrument working at 25 kV. Samples were analyzed as powders and prepared by deposition on aluminium sample holders followed by carbon coating using a Emitech K950 carbon evaporator. The average diameter of the nanoparticles was determined by analysis of HRTEM images using the software ImageJ v1.48 (at least 50 measurements for each case). GC-MS analysis were performed using a Hewlett Packard 5890 chromatograph equipped with a Mass Selective Detector MSD series II using helium as the carrier gas (35 cm s^{-1}); GC-FID was carried out in a Varian CP-3380 chromatograph to monitor the catalytic reactions. The

hydrogen was used as the carrier gas (55 cm s^{-1}) and fused silica Supelco capillary columns SPB-5 (30 m × 0.25 mm i.d.; 25 μm film thickness) were used.

Synthesis and preparation of the materials

$CoAl_2O_4$ nanoparticles. The nanoparticles were prepared through a non-aqueous sol-gel method following a recently published procedure.[32] The synthesis was carried out in a glovebox (O_2 and H_2O < 1 ppm). Briefly, in a glovebox, aluminium isopropoxide (2 mmol) was added to a cobalt acetate solution (1 mmol) in benzyl alcohol (20 mL) and allowed to stir for 10 min at room temperature. The mixture was then transferred to a stainless steel autoclave and placed in an oven for 2 days at 150 °C or 250 °C for the 2.5 nm and 5.5 nm nanoparticles, respectively. The suspension was centrifuged and the resulting solid was thoroughly washed with ethanol and dichloromethane, and dried in an oven at 60 °C.

Solid support MIL-101(Cr). The porous metal–organic framework (MOF) material was prepared by an adaptation of the method described by Férey *et al.*[14] Briefly, a mixture containing chromium(III) nitrate (2 mmol), benzene-1,4-dicarboxylic acid (2 mmol) and hydrofluoric acid (100 μL) in H_2O (10 mL) was stirred at room temperature for homogenization, transferred to an autoclave and heated at 220 °C for 9 h in an electric oven. After cooling to room temperature, the solid was recovered by centrifugation and purified through a double DMF and ethanol treatments.

Composite materials CoAl-*x*@MIL(Cr). The composite materials were prepared through the immobilization of the $CoAl_2O_4$ nanoparticles in the porous MIL-101(Cr). The nanoparticles (10 mg) were dispersed in ethanol (50 mL) and added to MIL-101(Cr) (240 mg). The mixture was stirred at room temperature for 24 h. Afterwards, the solid was isolated by centrifugation, washed thoroughly with ethanol and dried in a desiccator over silica gel. The incorporation with 5.5 nm and 2.5 nm nanoparticles lead to the formation of the CoAl-1@MIL(Cr) and CoAl-2@MIL(Cr) composites, respectively.

CoAl-1@MIL(Cr). Anal. found (%): Cr, 10.6; Co, 1.2; Al, 0.80; total metal loading: 2.0 wt%. Selected FT-IR (cm^{-1}): 3431, 1620, 1547, 1506, 1400, 1378, 1161, 1109, 1043, 1018, 885, 829, 748, 715, 660, 586. Selected FT-Raman (cm^{-1}): 3377, 3078, 1613, 1456, 1146, 868, 812, 631.

CoAl-2@MIL(Cr). Anal. found (%): Cr, 14.4; Co, 0.34; Al, 0.20; total metal loading: 0.54 wt%. Selected FT-IR (cm^{-1}): 3408, 1597, 1514, 1481, 1379, 1358, 1142, 1084, 1014, 991, 856, 806, 721, 688, 642, 565. Selected FT-Raman (cm^{-1}): 3080, 2934, 1615, 1460, 1148, 1044, 870, 812, 631.

Catalytic studies

The oxidation reactions (Scheme 1) were carried out in borosilicate 10 mL reaction vessels using acetonitrile (CH_3CN) as the solvent. In the oxidation of thioanisole (**i**), the substrate (0.5 mmol) and the catalyst [6 mg for CoAl-1@MIL(Cr) or 20 mg for CoAl-2@MIL(Cr)] were dissolved in CH_3CN (1.0 mL) under stirring and then H_2O_2 30% (2 mmol) was added to the reaction mixture. Regarding the oxidative reaction of styrene (**iv**), the substrate (1 mmol) and the catalyst (20 mg) were added to CH_3CN (1.5 mL) under stirring followed by the addition of aqueous *t*-BuOOH (4.5 mmol). All oxidative reactions were carried out at 70 °C. GC analysis was used to monitor the catalytic reactions and stopped when product yields remained constant after two successive GC analyses. An aliquot was taken directly from the reaction mixture with a microsyringe at regular intervals, diluted in acetonitrile and injected into the GC or GC-MS equipment for analysis of the starting material and products. The reaction products were identified by GC-MS analysis.

Acknowledgements

This work was partly financed by FEDER (Fundo Europeu de Desenvolvimento Regional) through COMPETE (Programa Operacional Factores de Competitividade) and by national funds through the FCT (Fundação para a Ciência e a Tecnologia) within the projects FCOMP-01-0124-FEDER-020658 (FCT ref. PTDC/EQU-EQU/121677/2010), FCOMP-01-0124-FEDER-013026 (FCT ref. PTDC/CTM/100357/2008), CICECO – FCOMP-01-0124-FEDER-037271 (FCT ref. PEst-C/CTM/LA0011/2013) and Requimte – FCOMP-01-0124-FEDER-037285 (FCT ref. PEst-C/EQB/La0006/2013), and the fellowships SFRH/BPD/73191/2010 (to CG) and SFRH/BPD/74477/2010 (to MK).

References

1 R. Ghosh Chaudhuri and S. Paria, *Chem. Rev.*, 2012, **112**, 2373–2433.
2 R. T. Kumar, N. C. Sagaya Selvam, T. Adinaveen, L. J. Kennedy and J. J. Vijaya, *React. Kinet., Mech. Catal.*, 2012, **106**, 379–394.
3 W. Xu, X. Liu, J. Ren, P. Zhang, Y. Wang, Y. Guo, Y. Guo and G. Lu, *Catal. Commun.*, 2010, **11**, 721–726.
4 C. R. Michel, *Sens. Actuators, B*, 2010, **147**, 635–641.
5 A. Dandapat and G. De, *ACS Appl. Mater. Interfaces*, 2012, **4**, 228–234.
6 W. Xu, X. Liu, J. Ren, H. Liu, Y. Ma, Y. Wang and G. Lu, *Microporous Mesoporous Mater.*, 2011, **142**, 251–257.
7 X. Wang, L. Liu and A. J. Jacobson, *Angew. Chem., Int. Ed.*, 2006, **45**, 6499–6503.
8 D. Maspoch, D. Ruiz-Molina, K. Wurst, N. Domingo, M. Cavallini, F. Biscarini, J. Tejada, C. Rovira and J. Veciana, *Nat. Mater.*, 2003, **2**, 190–195.
9 P. Horcajada, C. Serre, M. Vallet-Regí, M. Sebban, F. Taulelle and G. Férey, *Angew. Chem., Int. Ed.*, 2006, **45**, 5974–5978.
10 A. Corma, H. García and F. X. Llabrés i Xamena, *Chem. Rev.*, 2010, **110**, 4606–4655.
11 M. Meilikhov, K. Yusenko, D. Esken, S. Turner, G. Van Tendeloo and R. A. Fischer, *Eur. J. Inorg. Chem.*, 2010, **2010**, 3701–3714.
12 H. R. Moon, D.-W. Lim and M. P. Suh, *Chem. Soc. Rev.*, 2013, **42**, 1807–1824.
13 H.-L. Jiang and Q. Xu, *Chem. Commun.*, 2011, **47**, 3351–3370.
14 G. Férey, C. Mellot-Draznieks, C. Serre, F. Millange, J. Dutour, S. Surblé and I. Margiolaki, *Science*, 2005, **309**, 2040–2042.

15 C. M. Granadeiro, A. D. S. Barbosa, P. Silva, F. A. A. Paz, V. K. Saini, J. Pires, B. de Castro, S. S. Balula and L. Cunha-Silva, *Appl. Catal., A*, 2013, **453**, 316–326.
16 B. Yuan, Y. Pan, Y. Li, B. Yin and H. Jiang, *Angew. Chem., Int. Ed.*, 2010, **49**, 4054–4058.
17 Y. Huang, Z. Lin and R. Cao, *Chem.–Eur. J.*, 2011, **17**, 12706–12712.
18 J. Hermannsdörfer and R. Kempe, *Chem.–Eur. J.*, 2011, **17**, 8071–8077.
19 Y. Pan, B. Yuan, Y. Li and D. He, *Chem. Commun.*, 2010, **46**, 2280–2282.
20 S. S. Negi, K. Sivaranjani, A. P. Singh and C. S. Gopinath, *Appl. Catal., A*, 2013, **452**, 132–138.
21 M. Ghorbanloo, M. Jaworska, P. Paluch, G.-D. Li and L.-J. Zhou, *Transition Met. Chem.*, 2013, **38**, 511–521.
22 R. S. Walmsley, P. Hlangothi, C. Litwinski, T. Nyokong, N. Torto and Z. R. Tshentu, *J. Appl. Polym. Sci.*, 2013, **127**, 4719–4725.
23 N. Moussa, J. M. Fraile, A. Ghorbel and J. A. Mayoral, *J. Mol. Catal. A: Chem.*, 2006, **255**, 62–68.
24 M. R. Maurya, B. Singh, P. Adão, F. Avecilla and J. Costa Pessoa, *Eur. J. Inorg. Chem.*, 2007, **2007**, 5720–5734.
25 A. W. Jensen, B. S. Maru, X. Zhang, D. K. Mohanty, B. D. Fahlman, D. R. Swanson and D. A. Tomalia, *Nano Lett.*, 2005, **5**, 1171–1173.
26 G. A. B. Goncalves, S. M. G. Pires, M. M. Q. Simoes, G. Neves and P. Marques, *Chem. Commun.*, 2014, **50**, 7673–7676.
27 G. Li, H. Qian and R. Jin, *Nanoscale*, 2012, **4**, 6714–6717.
28 C. Chiappe, A. Sanzone and P. J. Dyson, *Green Chem.*, 2011, **13**, 1437–1441.
29 S. Ribeiro, L. Cunha-Silva, S. S. Balula and S. Gago, *New J. Chem.*, 2014, **38**, 2500–2507.
30 C. M. Granadeiro, P. Silva, V. K. Saini, F. A. A. Paz, J. Pires, L. Cunha-Silva and S. S. Balula, *Catal. Today*, 2013, **218–219**, 35–42.
31 M. M. Najafpour, M. Amini, D. J. Sedigh, F. Rahimi and M. Bagherzadeh, *RSC Adv.*, 2013, **3**, 24069–24074.
32 F. Rajabi, N. Karimi, M. R. Saidi, A. Primo, R. S. Varma and R. Luque, *Adv. Synth. Catal.*, 2012, **354**, 1707–1711.
33 S. Parihar, S. Pathan, R. N. Jadeja, A. Patel and V. K. Gupta, *Inorg. Chem.*, 2012, **51**, 1152–1161.
34 D. S. Gopala, R. R. Bhattacharjee, R. Haerr, B. Yeginoglu, O. D. Pavel, B. Cojocaru, V. I. Parvulescu and R. M. Richards, *ChemCatChem*, 2011, **3**, 408–416.
35 H.-F. Yao, Y. Yang, H. Liu, F.-G. Xi and E.-Q. Gao, *J. Mol. Catal. A: Chem.*, 2014, **394**, 57–65.
36 D. H. Lee, S. Kim, M. Y. Hyun, J.-Y. Hong, S. Huh, C. Kim and S. J. Lee, *Chem. Commun.*, 2012, **48**, 5512–5514.
37 M.-H. Xie, X.-L. Yang and C.-D. Wu, *Chem. Commun.*, 2011, **47**, 5521–5523.
38 S. S. Balula, C. M. Granadeiro, A. D. S. Barbosa, I. C. M. S. Santos and L. Cunha-Silva, *Catal. Today*, 2013, **210**, 142–148.
39 N. V. Maksimchuk, K. A. Kovalenko, S. S. Arzumanov, Y. A. Chesalov, M. S. Melgunov, A. G. Stepanov, V. P. Fedin and O. A. Kholdeeva, *Inorg. Chem.*, 2010, **49**, 2920–2930.
40 N. V. Maksimchuk, M. N. Timofeeva, M. S. Melgunov, A. N. Shmakov, Y. A. Chesalov, D. N. Dybtsev, V. P. Fedin and O. A. Kholdeeva, *J. Catal.*, 2008, **257**, 315–323.
41 S. H. Jhung, J. H. Lee, J. W. Yoon, C. Serre, G. Férey and J. S. Chang, *Adv. Mater.*, 2007, **19**, 121–124.
42 S. Ribeiro, C. M. Granadeiro, P. Silva, F. A. Almeida Paz, F. F. de Biani, L. Cunha-Silva and S. S. Balula, *Catal. Sci. Technol.*, 2013, **3**, 2404–2414.
43 O. V. Zalomaeva, K. A. Kovalenko, Y. A. Chesalov, M. S. Mel'gunov, V. I. Zaikovskii, V. V. Kaichev, A. B. Sorokin, O. A. Kholdeeva and V. P. Fedin, *Dalton Trans.*, 2011, **40**, 1441–1444.
44 M. Karmaoui, N. J. O. Silva, V. S. Amaral, A. Ibarra, A. Millan and F. Palacio, *Nanoscale*, 2013, **5**, 4277–4283.
45 Z. L. Li, J. H. Liu, C. G. Xia and F. W. Li, *ACS Catal.*, 2013, **3**, 2440–2448.
46 L. Bromberg, Y. Diao, H. Wu, S. A. Speakman and T. A. Hatton, *Chem. Mater.*, 2012, **24**, 1664–1675.
47 S. K. Karmee, L. Greiner, A. Kraynov, T. E. Muller, B. Niemeijer and W. Leitner, *Chem. Commun.*, 2010, **46**, 6705–6707.
48 W. Wang, Y. Xu, D. I. C. Wang and Z. Li, *J. Am. Chem. Soc.*, 2009, **131**, 12892–12893.
49 V. R. Choudhary, D. K. Dumbre, N. S. Patil, B. S. Uphade and S. K. Bhargava, *J. Catal.*, 2013, **300**, 217–224.
50 Y. Liu, H. Tsunoyama, T. Akita and T. Tsukuda, *Chem. Commun.*, 2010, **46**, 550–552.
51 N. Linares, C. P. Canlas, J. Garcia-Martinez and T. J. Pinnavaia, *Catal. Commun.*, 2014, **44**, 50–53.